EFDA–JET–PR(10)47

S. Moradi, C. Bourdelle, M.Z. Tokar, X. Litaudon, F. Imbeaux, Y. Corre,
P. Monier-Garbet, D. Kalupin, B.Weyssow
and JET EFDA contributors

Modeling of Energy Confinement Improvement in High Power JET Discharges with Neon Seeding

Modeling of Energy Confinement Improvement in High Power JET Discharges with Neon Seeding

S. Moradi[1], C. Bourdelle[2], M.Z. Tokar[3], X. Litaudon[2], F. Imbeaux[2], Y. Corre[2], P. Monier-Garbet[2], D. Kalupin[4], B.Weyssow[4]
and JET EFDA contributors*

JET-EFDA, Culham Science Centre, OX14 3DB, Abingdon, UK

[1]Department of Applied Mathematics, Nuclear Engineering, Chalmers University of Technology, SE-412 96 Göteborg, Sweden
[2]CEA, IRFM, F-13108 St Paul Les Durance, France.
[3]Institut für Energieforschung - Plasmaphysik, Forschungszentrum Jülich, Association EURATOM-FZJ, Trilateral Euregio Cluster, Germany
[4]EFDA-CSU Garching, München Germany
** See annex of F. Romanelli et al, "Overview of JET Results", (23rd IAEA Fusion Energy Conference, Daejon, Republic of Korea (2010).*

Preprint of Paper to be submitted for publication in
Nuclear Fusion

ABSTRACT

In order to reduce the heat load to the wall, in particular in presence of a metallic wall, the radiated fraction is increased by means of impurity seeding. The present paper aims at investigating qualitatively the balance between a degradation of the edge confinement and a potential reduction of the core turbulent transport due to the increase of effective charge, Z_{eff} . The pedestal degradation due to the Ne seeding is taken as input. The impact of Z_{eff} and radiative loss on the heat transport are modeled with the quasi-linear 1-D fluid code RITM. The input parameters are taken from a series of Ne seeded discharges conducted in JET. Discharges with D, D+Ne and Ne only fueling are qualitatively analyzed. The model recovers the experimentally observed fact that, while the confinement is degraded from the D to the D +Ne seeded plasma, it is improved from the D+Ne to the Ne only seeded plasma.

1. INTRODUCTION

To reach regimes compatible with reasonable heat loads to the wall, there are several constraints which should be overcome simultaneously [1]; some of the main constraints can be listed as:

(1) to control and reduce both stationary and transient heat loads on the plasma facing components;
(2) a high level of radiated power in the divertor and
(3) avoiding impurity accumulation in the core.

One of the most severe problems for fusion reactors is to satisfy the technological constraint imposed by the divertor target Plasma Facing Components (PFCs). However, strong ELM activity can lead to power loads in excess of technically acceptable levels. In order to reduce ELM activity, different techniques are used. By increasing the radiated fraction the ELM activity can be reduced. Increased D fueling will lead to increase of the electron density in the SOL, and therefore the radiation from intrinsic impurities such as carbon. With D fueling alone, up to 40-45% [2, 3, 4, 5] of the total injected power can be radiated. To go above 40-45% extrinsic impurities have to be seeded. Radiation cooling experiments with extrinsic impurities have been performed on several tokamaks [6, 7, 8, 9, 10] in order to reduce the heat flux to the plasma facing components among which limiters and divertors. Increased radiation can lead to a pedestal degradation as seen systematically at JET [1, 2, 3, 4, 5] or no pedestal modification as seen in ASDEX Upgrade [11]. The seeded impurity is chosen to optimize the radiation in the SOL. However, some penetrate in the plasma core, which can lead to radiation from core and also dilution. These effects, in terms of core impurity content, can lead to a reduction of fusion performance which is not desirable for a tokamak reactor.

There is a variety of results of seeding impurities on the confinement properties. Both confinement degradation and improvement have been observed in L and H mode discharges. Some of the examples of such a variety can be summarized as followed:

- Degradation of the energy confinement time τ_E:
  - The results reported by M. Beurskens [2] show that at JET H-mode when injecting Ne and at $P_{rad} > 50\%$ the pedestal pressure is degraded by at least 25% and there is no sign of improved core confinement. At high radiation levels, the ELMs are of type III, and these lead to reduction of both transient and stationary heat loads. The total combined input power ($P_{tot} = P_{NBI} + P_{ICRH} + P_{Ohm}$) for the plasmas in these experimental series was between 20 and 25MW.

- Improvement of the energy confinement time τ_E:
  - The results reported by Y. Corre [3] where N seeding for ELM mitigation in JET hybrid discharges were performed, show that when injecting N and at Prad ≥ 40% even though the confinement is reduced by about 20% comparing to the discharges without N seeding (with the same D fueling), when increasing N content and consequently Prad, the confinement is stabilized or even slightly improved. In these experiments the averaged total injected power was around 20MW. Such a plasma behavior at JET is also seen in the results reported by X. Litaudon [1] in high power discharges with $P_{NBI} = 22$MW and the total power, including ohmic heating, of 30MW. Here, it is observed that by seeding Ne the radiation fraction is increased to up to $P_{rad} \geq 60\%$ and as a result the electron pedestal pressure was decreased by about 20 to 30%. However, with a stronger Ne fueling rate the confinement was improved and it was seen that the fusion performance in terms of neutron yield rate remained the same as that in the discharge without Ne seeding. These discharges are the subject of this study.
  - In ASDEX Upgrade improved confinement in L-mode discharges has been obtained by injecting Ne impurities at power levels between 1 and 10MW, as reported by J. Neuhauser [12]. By increasing the radiated power the confinement increased and, at high radiation powers, reached 80% of that of the H-mode.
  - The results reported by G. Tardini [11] show that in ASDEX Upgrade H-mode discharges a systematic confinement improvement by N seeding is obtained. Here, the pedestal confinement was improved and no significant enhancement of the core confinement was observed.

These results show that optimum plasma parameters to solve the problem of heat exhaust may not be optimum for core confinement, and that the impact of fueling in the SOL and pedestal is not understood since different machines can have different pedestal responses to the impurity seeding. As a consequence the non-linear interplay between edge and core plasma is a key issue in present tokamak.

In this paper, heat transport modeling of JET discharges with Ne seeding reported in Ref. [1], as mentioned above, are presented. The modeled discharges were part of a series of experiments at JET aimed to explore the operation at high power in configurations relevant to ITER steady-state

scenarios, where in order to increase the edge radiation high-Z radiative gas, such as Ne, were injected into the plasma. To model the heat transport we use the fluid code RITM [13, 14, 15, 16], and we restrict our modeling inside the LCFS. This is mostly because in the SOL, modelling of the turbulent transport coupled to radiative processes is extremely difficult and at present there is no satisfactory way to do that. The boundary conditions are given by the measured temperatures at $\rho = 1$. In the present study, the particle transport is not modeled, since the cause for the loss of the pedestal electron density observed in these discharges, is not well understood and in order to simplify the problem only heat transport is computed. Therefore, we will focus on the balance between: the increased radiation level inside the LCFS, the increased Ne concentration and the modified confinement. The experimental observations are shown in section 2. In section 3, the model used is described as well as the frame in which it is used for the present study. In section 4, the results obtained are presented and discussed. In section 5, conclusions are drawn.

2. EXPERIMENTAL OBSERVATIONS

During 2006-2007 JET experimental campaigns, a series of discharges was dedicated to explore the operation at high power in configurations relevant to ITER steady-state scenarios. In these discharges, Ne seeding has been explored to increase the radiated power fraction, providing significant reduction of target tile power fluxes and mitigation of ELM activities. A high confinement was observed for the reference Pulse No: 69089, where only D fueling was applied, however, the radiated power fraction was only about 20% and with type I ELMs. In two Ne seeded Pulse No's: 69091 with D and Ne seeding, and 69093 with only Ne seeding, the radiated power fraction was increased to similar values of up to 60%. The pedestal confinement was reduced in comparison with the non seeded discharge. A stronger Ne puffing in Pulse No: 69093 was performed in order to mitigate ELM affecting detrimentally the internal transport barrier to develop an Advanced Tokamak (AT) scenario at high triangularity. In this discharge, the Ne content was almost double than that in discharge 69091, and the amplitude of the ELM perturbation was strongly reduced [2]. The diamagnetic stored energy was increased by 25% and this performance improvement was seen on the ion temperature profiles which showed a temperature increase both at the top of the H-mode pedestal and in the core (from 6 to 12keV). The electron density, also, increased by ~10 % in the core. The neon concentration profile, as measured by the charge exchange recombination spectroscopy, was hollow with a concentration of about 1% in the core rising to ~2.5% at the normalized radius of 0.7 [1]. No sign of impurity accumulation was found in this discharge. The cause of the improvement was not identified, however, comparison between the three discharges suggests that with further increased Ne content, the confinement degradation appears to have stopped and reverted to better confinement [1, 2, 3].

In the Ne seeded discharges, the Ne puffs were different only during the initial phase with a short strong burst of about a factor of two higher in Pulse No: 69093 than that in Pulse No: 69091. Nearly the same waveform as in Pulse No: 69091 was used thereafter. The D_α puff intensity has

been 6 times higher for the Pulse No: 69091 than for Pulse No: 69093. However, the pedestal electron densities are similar for the two Ne seeded discharges. Because the particle transport and loss processes of the fueled species from the wall to LCFS are not well understood, the reason for this similarity in the pedestal electron densities, even though the fueling rates are very different is not understood. Hence, in the present study we fix the density profiles to their experimental values and do not model particle transport.

All discharges in question have been heated with a high NBI power of 22MW and a total power, including ohmic heating, of 30MW; the magnetic field $B_0 \sim 3.1$ T, plasma current $I_P \sim 1.9$MA, triangularity $\delta \geq 0.3$. These AT scenarios are characterized by q_{95} of about 5, operation at relatively high normalized $\beta_N \sim 2$, and a flat q profile (sometimes hollow) with a minimum q of about 1.5-2.5. A summary of plasma parameters for the three considered discharges is given in the table 1. In this table, the values of the energy confinement time τ_E are calculated by assuming $P_{tot} = 30$MW for all three discharges and using W_{th} computed by subtracting the contributions of the super-thermal particles from EFIT W_{Dia} data. The total radiated power inside LCFS, P_{rad}^{inLCFS}, is taken from JET database. These values show that τ_E is comparable for non seeded Pulse No: (69089) to that from low Ne content Pulse No: (69091) while it is the highest in the high Ne content Pulse No: (69093).

Figures 1 to 7 show the experimental values of the plasma parameters taken from JET database. The total radiated powers P_{rad}^{tot}, from LCFS + SOL regions are given in table 1. Figure 1 shows P_{rad}^{tot} versus time taken from JET 2D tomographic reconstruction, for the three considered discharges.

Figure 2 shows the total radiated power profiles, P_{rad}^{inLCFS} , as a function of normalized flux, Ψ, inside LCFS taken from measurements based on Abel inversion (reconstruction under assumption that plasma radiation is constant on the flux surface). The radiated power is calculated by integrating with the time step $\delta t = 0.1$s (between ELMs) from t = 5s until 9.9s. As seen in this figure the radiated power inside LCFS is higher for the discharge with high Ne content (69093) than the other two discharges. The ratio between the total radiated power and radiated power from the main plasma (inside LCFS), $P_{rad}^{inLCFS}/P_{rad}^{tot}$ is given in table 1 which indicates that with higher Ne seeding (69093) the total radiated power inside the LCFS has increased. This is due to the fact that the ionization depth for Ne is larger than that for the intrinsic impurities such as C, and therefore some Ne neutrals can penetrate inside LCFS and increase the radiation there.

Figure 3 shows the T_i profiles taken from the charge exchange (CXRS/CXFM) diagnostic measurements and, figures 4, 5 show T_e, n_e profiles taken from the Thomson scattering (LIDAR) diagnostic measurements, for these series of experiments, the High Resolution Thomson Scattering measurements [17] were not available. As seen in figures 3 and 4 the ion and electron temperatures are almost identical for two Pulse No's: 69089 and 69091 but they increase significantly (almost double for Ti) in Pulse No: 69093 at all plasma radius.

Comparing the pedestal electron density profiles there is a decrease from the Pulse No: 69089 (without Ne seeding) to the two seeded discharges.

Although the D fueling intensity has been 6 times higher for the Pulse No's: 69091 than for

69093 as seen in figure 5, the electron density profiles differ from only 20% in the core and are almost identical in the pedestal. The reason for such similarities in electron density profiles is not known since, the particle transport and loss mechanisms of the fueled species in the SOL are not understood.

Figures 6 and 7 illustrate C and Ne concentration profiles for the three discharges and figure 8 shows the associated Z_{eff} profiles calculated by taking into account both C and Ne (when present) impurities. These data are taken from charge exchange measurements. As seen in figure 7 a reduction of the carbon concentration down from 3% in the non seeded Pulse No: (69089) to 1% (at R = 3.6 m) in the seeded Pulse No: (69093) is observed.

3. FRAMEWORK IN WHICH THE TRANSPORT MODELING IS APPLIED

In order to investigate the underlying mechanisms responsible for the observed plasma behaviors in the discharges mentioned above we perform a qualitative transport modeling in a series of tests. For transport modeling the quasi-linear 1-D fluid transport code RITM [13, 14, 15, 16], has been applied.

In general, the RITM code allows a self-consistent description of heat and particle transport over the entire cross section of the plasma from the axis to the separatrix. Continuity equations are solved separately for electrons and impurity ions in all ionization stages and the density of the background ions is calculated under the assumption of plasma quasi-neutrality.

The goal of the present study is to model only the plasma behavior inside the separatrix, hence excluding the SOL. Although the modifications in the SOL, from one discharge to another can have a great impact on the behavior of the plasma, we do not take them into account here, because of the limited ability to model turbulence, particle sources and the radiative processes in the SOL.

The pedestal degradation observed on density at JET is not presently well understood, therefore the particle transport is not modeled. The pedestal density degradation is taken as an input information. Only the heat transport and the radiation levels inside LCFS are computed by RITM. The impact of the impurities on the transport is taken into account by assuming that there are two plasma species: electrons and an effective ion with an effective charge, Z_{eff} . Therefore, the presence of impurities affect the plasma through: 1) the modification of Z_{eff} which is prescribed from the Modeling of energy confinement improvement in high power JET discharges with neon seeding experimental profiles (see figure 8), and 2) their radiations.

The radiation profile is computed only inside the LCFS by taking both C and Ne radiations in all ionization states. The experimental Z_{eff} and the total radiated power inside LCFS, P_{rad}^{inLCFS} are used as constraints for these calculations. Radiations from fueled particles (D) are not considered since D_α is mostly in the SOL. No boundary constraint on the value of P_{rad}^{inLCFS} ($\rho = 1$) is assumed. The radiated power profiles together with the experimental profiles of auxiliary heating power density from the NBI and high frequency radio-waves are taken from JET database, and are used in the ion and electron heat transport equations to calculate the radial temperature profiles.

Unfortunately, the High Resolution Thomson Scattering measurements were not available for

these series of discharges however, a reduction in the pedestal density under similar conditions was also observed when this diagnostic was available, see Ref. [2]. Therefore, to account for highest reduction of density in our computations we have simply assumed the highest pedestal reduction from (Pulse No: 69093) together with the highest core density reduction from (Pulse No: 69091) (see figure 5). The boundary conditions for temperatures, T_i and T_e at $\rho = 1$ are defined using the experimental values taken from edge Charge eXchange SpEctroscopy (CXSE) and interferometer (KK1,KK3) measurements, respectively (see figures 3, 4). The safety factor, q_{sf} , profiles are fixed by the calculated values taken from EFIT data coherent with an EFIT constraint by MSE. A summary of the parameters fixed to the experimental data and modeled by RITM is given in table 2.

4. RESULTS OF THE MODELING

Starting from the discharge with only D fueling (Pulse No: 69089), towards the discharges with Ne seeding, the expected impacts on the confinement are: a degradation due to the density reduction, a degradation due to P_{rad}^{inLCFS} increase, and an improvement due to Z_{eff} increase. In order to balance these three effects, the impact of each is first modeled separately, namely:

(1). The impact of the pedestal density modification (inside LCFS) from Pulse No's: 69089 to 69091 – 3 is shown in figure 9 following the red star to the green diamond. A density decrease and therefore, a density gradient increase at the edge (at the last 10% of the normalized radius), as seen in figure 5 leads to on the one hand, an increase of the Trapped Electron (TE) modes, and on the other hand some stabilization of the Ion Temperature Gradient (ITG) modes. Therefore, the overall temperatures did not vary strongly, and it is simply the density reduction that affects the confinement time following the relation: Energy = $3/2 \int dV\, nT$. About 25% decrease in E is observed as one would expect for a density decrease seen in figure 5.

(2) The impact of an increase of Z_{eff} from Pulse No: 69089 to the Pulse No's: 69091 and 69093 on the confinement time is shown in figure 9 following the red star to the crayon and pink diamonds, respectively. A more pronounce increase of about 25% is observed from the Pulse No's: 69089 to 69093. The causes for this increase can be understood by analyzing the figure 10 where the radial profiles of the corresponding ITG growth rates are shown. One can interpret this evolution by taking into account that the main contribution to the anomalous part in heat diffusivity $\chi_{i,e}$ is due to ITG instability [18]. This contribution is determined by the ITG growth rate as

$$\gamma_{ITG} \sim \sqrt{\frac{1}{Z_{eff} L_{Ti}} - \frac{1}{L_{Ti}^{cr}}} \qquad (1)$$

where L_{Ti} and L_{Ti}^{cr} are the e-folding length of the ion temperature and its critical value, correspondingly. In the plasma core T_i-profile is stiff, i.e., $Z_{eff} L_{Ti} \approx L_{Ti}^{cr}$ and for relatively

flat density $L_{Ti}^{cr} \approx \alpha R$. With a constant Z_{eff} we get $T_i(0)/T_i(r_b) \approx \exp(Z_{eff}\, r_b/\alpha R)$ where rb is the minor radius corresponding to the plasma boundary i.e., at $\rho = 1$. This temperature ratio grows up with increasing Z_{eff} . Figure 11 shows T_e and T_i profiles corresponding to Z_{eff} increase shown in figure 9 following the red star to the crayon and pink diamonds.

(3) The increase of radiated power, P_{rad}^{inLCFS}, inside the LCFS on the confinement time is estimated, see figure 9 following the red star to the orange diamond. A degradation of the confinement due to the cooling of the electrons is expected, however, a very weak degradation is found. This weak degradation is explained by the very small reduction of T_e and T_i profiles shown in figure 12. It seems that in our model such an increase of radiated fraction (about 20% increase) does not generate strong effect on the electron temperature, and its impact on the anomalous electron heat transport through modifications of T_e and ∇T_e remains negligible. The modification of T_e and ∇T_e due to radiation however, may increase if a more accurate radiative loss model is used.

After investigating each individual effect on the confinement time, now we will balance them. We know that both the density reduction and increase in P_{rad}^{inLCFS} lead to confinement degradation whereas increase of Z_{eff} leads to confinement improvement. On the one hand, degradation of the confinement due to the increased radiated power is weak and if balanced against the increase of Z_{eff} the impact of Z_{eff} is stronger and it leads to an improved confinement (see figure 9 following the orange to brown diamond). This effect has been previously observed in the RI modes. On the other hand, the impact of the decreased pedestal density compared to the improvement due to the increased Z_{eff} shows that the impact of density reduction can be to some extend compensated by the increase of Z_{eff}, (in figure 9 by going from purple diamond to black star). This effect can be seen also on the electron and ion temperature profiles shown in figure 13, corresponding to the red star and brown diamond in figure 9. These trends are qualitatively coherent with experimental observations when comparing the values of normalized β (calculated using W_{th} values computed by subtracting the contributions of the super-thermal particles from EFIT W_{Dia} data) where: for the Pulse No: 69089 is around 1.6, for Pulse No: 69091 is 1.5 and for Pulse No: 69093 is around 1.9.

Here, we would like to recall that due to error bars on the experimental measurements of the density and temperatures, the aim of the present study is only to qualitatively analyze the observed plasma behaviors and we make no quantitative judgments on the computed values. The modeled behavior agrees qualitatively with the experimental observation. Hence, one can expect that there exist a critical value of Z_{eff} above which the degradation of the pedestal is counter balanced by the improvement due to a higher Z_{eff}. The critical Z_{eff} will vary depending on the background dimensionless parameters. In the studied case here, this value is between Z_{eff} measured for Pulse No's: 69091 and 69093, i.e. between 2 and 3. In such a picture, the results reported by M. Beurskens [2] showing mostly degradation of the confinement with impurity seeding can be compatible with other reported results showing an improvement of the confinement with impurity seeding in JET H-mode and ASDEX Upgrade [3, 1, 12, 11].

CONCLUSIONS

We have performed a qualitative transport modelling of the JET discharges where Ne seeding has been explored to increase the radiated power fraction (up to 60%), providing a significant reduction of target tile power fluxes (and hence temperatures), and mitigation of ELM activities. For transport modeling the one-dimensional fluid transport code RITM has been applied. We have investigated the observed plasma behavior in a series of tests and the obtained results show that the interplay between the edge and core confinement is very delicate. By decreasing the plasma pressure at the edge in order to reduce the ELM activities, the edge confinement always degrades. The degradation of the confinement due to the increased radiated power alone is weak, and if balanced against the increase of Z_{eff} the stabilizing impact of Z_{eff} can be stronger. Therefore, the edge confinement can be compensated by the increase of the core confinement. This core confinement improvement can be achieved by an increase in Z_{eff} through its impact on suppressing the core ITG instability. However, the degrading impact of the decreased pedestal density balanced against the improvement of the core confinement by increased Z_{eff}, indicates that the impact of density reduction is stronger [than improvement with Z_{eff}] when going from Pulse No's: 69089 to 69091. By further increase of Z_{eff} in Pulse No: 69093, the degraded pedestal confinement is completely compensated by the improved core confinement and the overall confinement is even improved in comparison to the non seeding discharge (69089). A summary of the obtained results is given in table 3. These results can reproduce qualitatively the experimental observations [1].

Increasing impurity concentration can have two types of impacts: 1) degradation of confinement through radiative losses in the case of the Pulse No: 69091, and also discharges shown in the reference [2] with lower input power, P_{tot} = 20–25MW, where the increase in Z_{eff} is not able to generate high enough core confinement so as to compensate for the radiative losses at the edge. 2) The overall confinement recovery can occur in the case of discharge 69093 where Z_{eff} is higher and leads to improved core confinement enough so as it compensates the degraded edge and it can possibly even further improve by further increasing Z_{eff} . Some examples where the improved confinement by increase of Zeff is seen: at JET in the reference [3] where nitrogen seeding for ELM mitigation in hybrid discharges were performed, and the improved Lmode regime of ASDEX-Upgrade [12]. While the edge improved confinement in N seeded H-mode discharges at ASDEX-Upgrade [11] is shown to be the reason for improved confinement at JET however, a pedestal density degradation has been observed in Ne seeded H-mode discharges and an improved core confinement from the present simulation is expected to explain the improved confinement. Hence, at yet there is no unified model that can explain both observations, and this should be the aim of future works, i.e. 1) the impact of the background parameters on the critical Z_{eff} value should be investigated, and 2) the pedestal and core should be modelled simultaneously.

ACKNOWLEDGMENTS

This work, supported by the European Communities under the contract of Association between

the EURATOM-VR Sweden and the EURATOM/CEA Association, was carried out within the framework of the European Fusion Development Agreement. The views and opinions expressed herein do not necessarily reflect those of the European Commission.

REFERENCES

[1]. Litaudon X et al 2008 Plasma Physics and Controlled Fusion **49** B529-B550
[2]. Beurskens M.N.A et al 2008 Nuclear Fusion **48** 095004
[3]. Corre Y et al 2008 Plasma Physics and Controlled Fusion **50** 115012
[4]. Jachmich S et al 2002 Plasma Physics and Control Fusion **44** 1879-1891
[5]. Rapp J et al 2009 Nuclear Fusion **49** 095012
[6]. Ongena J et al 2001 Physics. Plasmas **4** 2188
[7]. Dominguez R.R. and Waltz R.E 1987 Nuclear. Fusion **27** 65
[8]. Lazarus E.A. et al 1984 Journal and Nuclear Materials **121** 61
[9]. Kubo K et al 2001 Nuclear Fusion 41 227
[10]. Matthews G.F. et al 1999 Nuclear Fusion **39** 19
[11]. Tardini G et al 2010 Core transport and pedestal characteristics of nitrogen seeded H-mode discharges in ASDEX Upgrade Proceedings of the 37th EPS Conference on Plasma Physics P1. 1097
[12]. Neuhauser J. et al 1995 Plasma Physics and Control Fusion **37** A37
[13]. Tokar M.Z. 1994 Plasma Physics and Control Fusion **36** 1819
[14]. Unterberg B et al 2004 Plasma Physics and Control Fusion **46** A241
[15]. Kalupin D et al 2005 Nuclear Fusion **45** 468
[16]. Moradi S et al 2008 Modeling of confinement improvement and impurity transport in high power JET H-mode discharges with neon seeding Proceedings of the 35th EPS Conference on Plasma Physics
[17]. Pasqualotto R et al 2009 Review of Scientific Instruments **75** 3891
[18]. Tokar M.Z. et al 1999 Plasma Physics and Control Fusion **41** L9

	D [el/s]	N_e [el/s]	P_{rad}^{tot}	$\frac{P_{rad}^{inLCFS}}{P_{rad}^{tot}}$	$\tau_E = \frac{W_{th}}{P_{tot} - P_{rad}^{inLCFS}}$
69089	0.5×10^{22}	-	20%	38%	0.140
69091	3×10^{22}	3.8×10^{21}	60%	56%	0.145
69093	0.5×10^{22}	6.3×10^{21}	60%	63%	0.160

Table 1: A summary of plasma parameters.

Experimental data constraining the model	*Data modeled in RITM*
$q(\rho)$	*Heat Transport:* $\chi_{i,e}(\rho)$
$T_{e,i}(\rho = 1)$	*Temperature profiles:* $T_{e,i}(\rho)$
$n_e(\rho)$	*Radiation profile:* $P_{rad}^{inLCFS}(\rho)$*: (radiation*
$Z_{eff}(\rho)$	*from C and Ne while their concentration*
Total radiated level inside LCFS	*is constraint by*
Auxiliary heating power density (NBI and RF)	*experimental* $Z_{eff} = C + Ne$*)*

Table 2: A summary of the parameters fixed to experimental data and modeled by RITM.

	P_{rad}^{inLCFS} *increase*	P_{rad}^{inLCFS} *increase + pedestal density degradation*	P_{rad}^{inLCFS} *increase + pedestal density degradation + moderate* Z_{eff} *increase (69091)*	P_{rad}^{inLCFS} *increase + pedestal density degradation + stronger* Z_{eff} *increase (69093)*
τ_E *(at high* P_{rad}*)* / τ_E *(at low* P_{rad}*)*	*Weak impact (red start to orange diamond)*	*< 1 (red star to purple diamond)*	*< 1 (red to black star)*	*< 1 (red to blue star)*

Table 3: A summary of the obtained results by RITM.

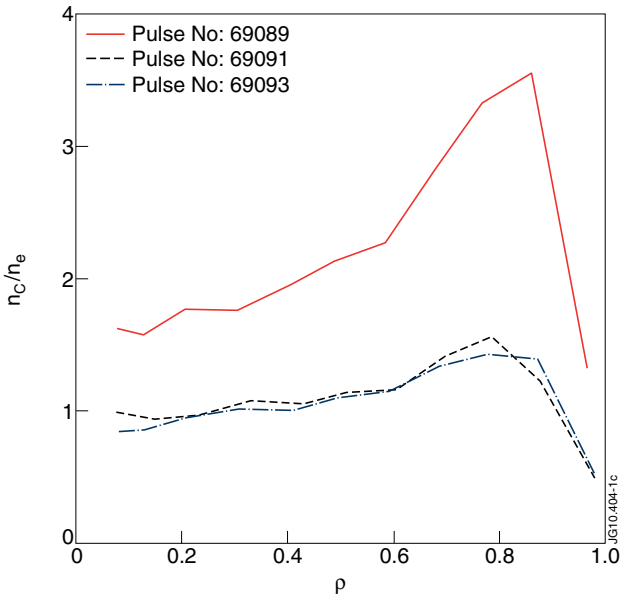

Figure 1: P_{rad}^{tot} total radiated power as a function of time (taken from JET measurements base on 2D tomographic reconstruction) for the three Pulse No's: 69089 (solid line), 69091 (dashed line) and 69093 (dashed dotted line).

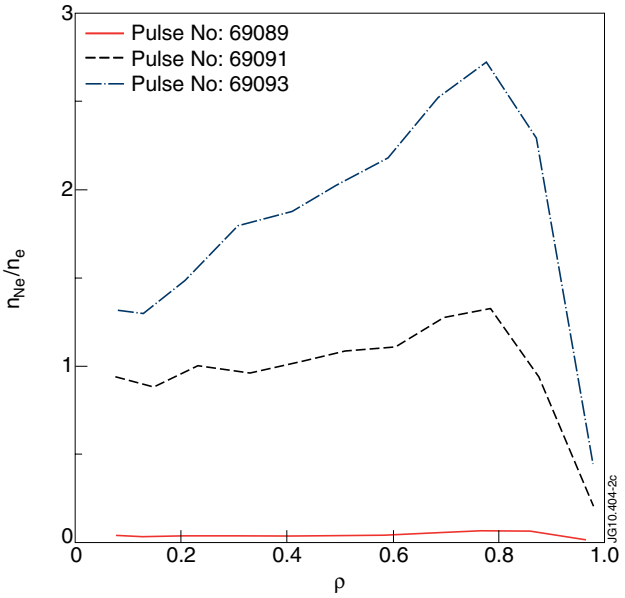

Figure 2: P_{rad}^{inLCFS} total radiated power within flux surfaces (inside LCFS) as a function of normalized flux, Ψ, taken from JET measurements based on Abel inversion (reconstruction under assumption that plasma radiation is constant on the flux surface) for the two discharges at t ≈ 7.6s: 69091 (dashed line) and 69093 (dashed dotted line).

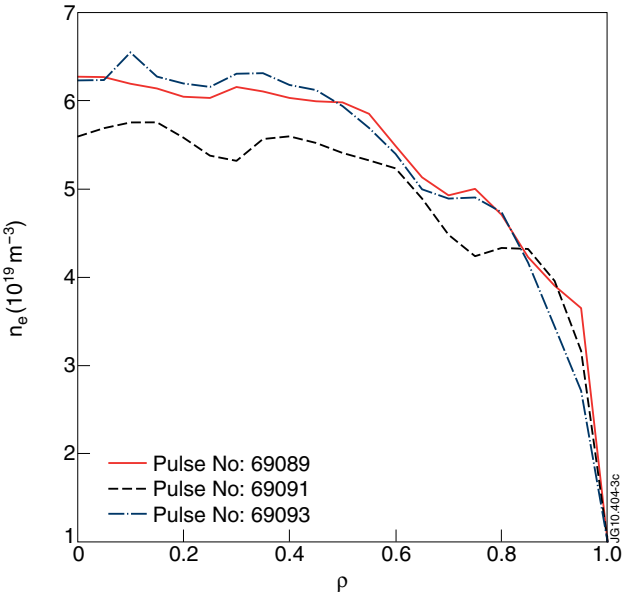

Figure 3: T_i profiles as functions of normalized radius (taken from JET CXFM measurements) for the three discharges at t ≈ 7.6s: 69089 (solid line), 69091 (dashed line) and 69093 (dashed dotted line).

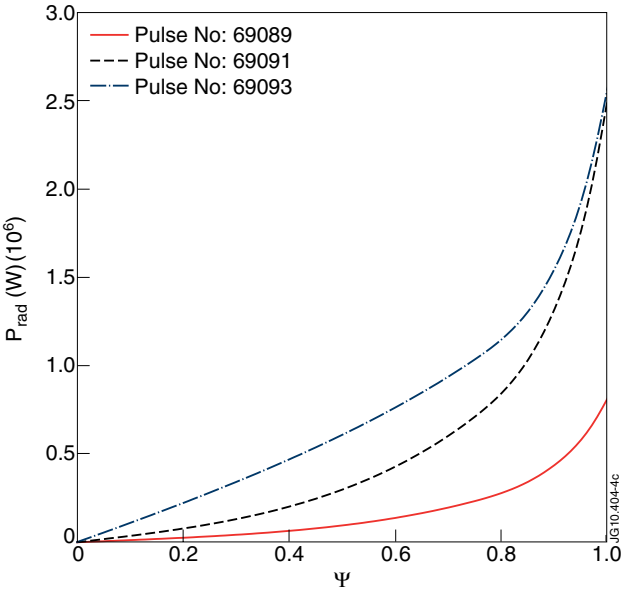

Figure 4: T_e profiles as functions of normalized radius (taken from JET LIDAR measurements) for the three discharges at t ≈ 7.6s: 69089 (solid line), 69091 (dashed line) and 69093 (dashed dotted line).

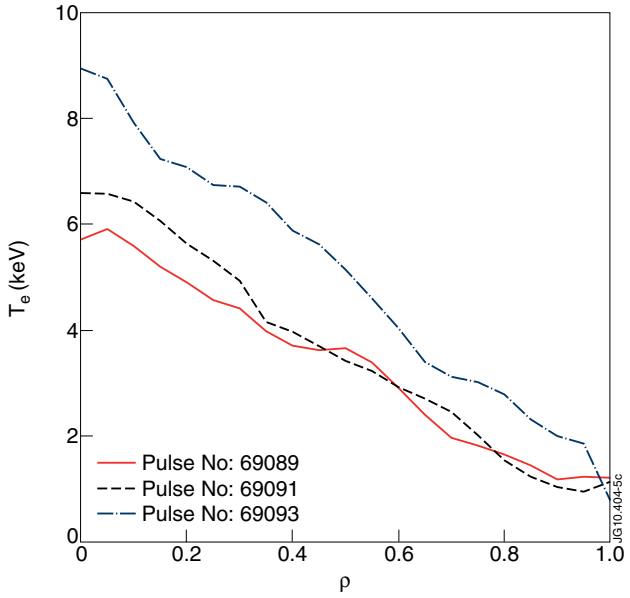

Figure 5: Electron density n_e profiles as functions of normalized radius (taken from JET LIDAR measurements) for the three discharges at t ≈ 7.6s: 69089 (solid line), 69091 (dashed line) and 69093 (dashed dotted line).

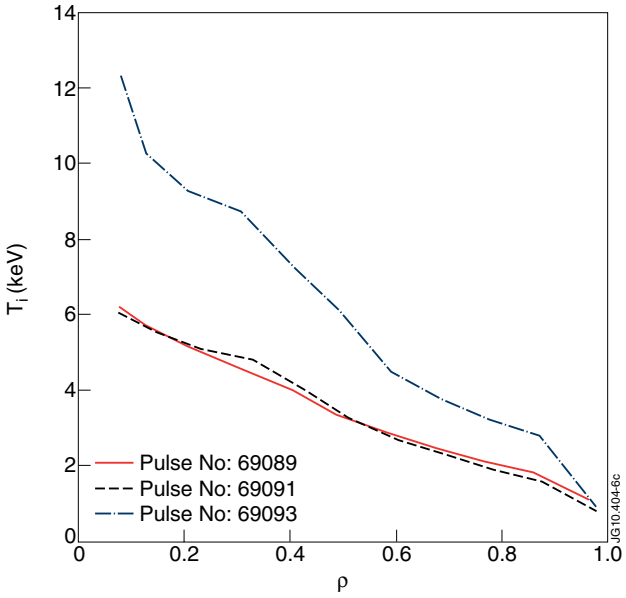

Figure 6: Neon concentration, n_{Ne}/n_e profiles as functions of normalized radius (taken from JET charge exchange recombination spectroscopy measurements) for the three discharges at t ≈ 7.6s: 69089 (solid line), 69091 (dashed line) and 69093 (dashed dotted line).

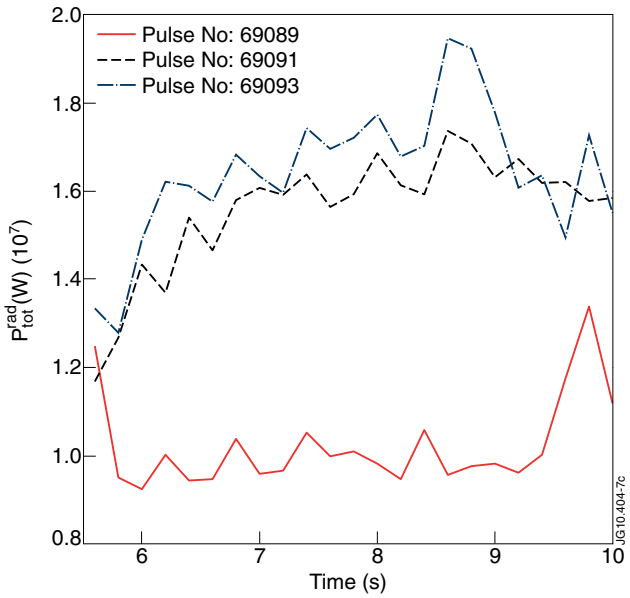

Figure 7: Carbon concentration, n_C/n_e profiles as functions of normalized radius (taken from JET charge exchange recombination spectroscopy measurements) for the three discharges at t ≈ 7.6s: 69089 (solid line), 69091 (dashed line) and 69093 (dashed dotted line).

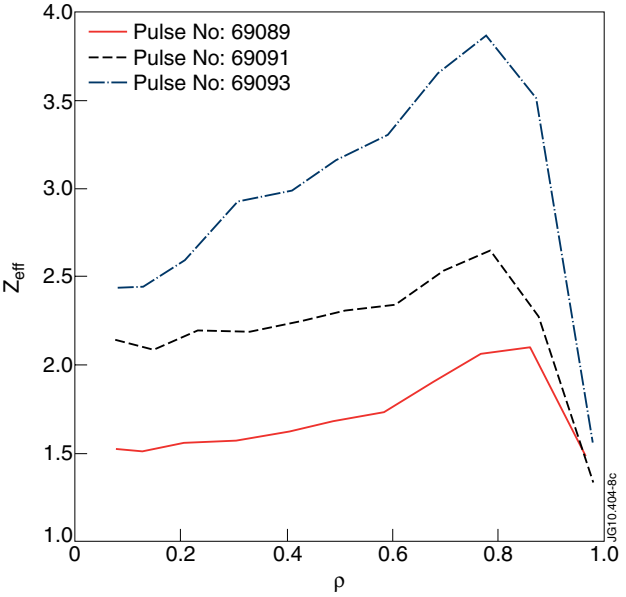

Figure 8: Effective charge, Z_{eff} profiles as functions of normalized radius (taken from JET charge exchange recombination spectroscopy measurements) for the three discharges at t ≈ 7.6s: 69089 (solid line), 69091 (dashed line) and 69093 (dashed dotted line).

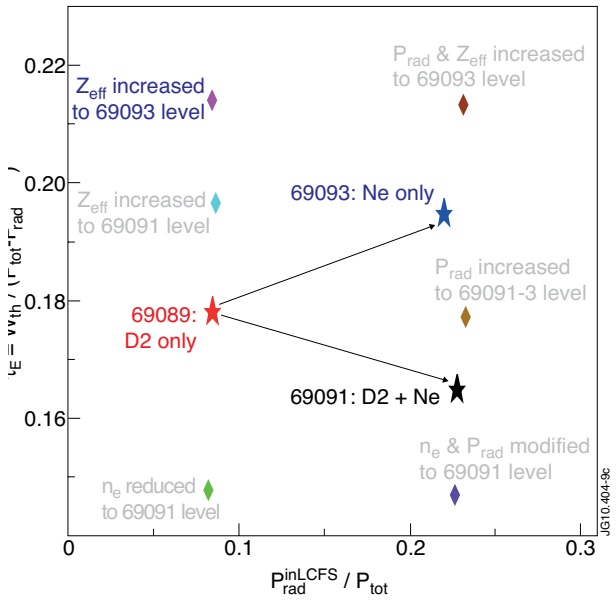

Figure 9: The energy confinement time defined as the ratio of the diamagnetic energy to the total input power: $\tau_E = W_{th}/(P_{tot} - P_{rad}^{inLCFS})$ versus the fraction of radiated power, P_{rad}^{inLCFS} /Ptot for different tests. The reference discharge 69089 with only D fueling is shown with a red star. The other two discharge: 69091 (D fueling and Ne injection) and 69093 (only Ne injection) are presented by a black and blue stars, respectively. Diamond symbols represent the tests where only n_e (green), only Z_{eff} of 69091 (crayon), only Z_{eff} of 69093 (pink), only P_{rad}^{inLCFS} (orange) and finally, P_{rad}^{inLCFS} $+n_e$ (purple), P_{rad}^{inLCFS} $+Z_{eff}$ (brown) have been replaced from their reference values in 69089 by those from 69091 – 3 discharges.

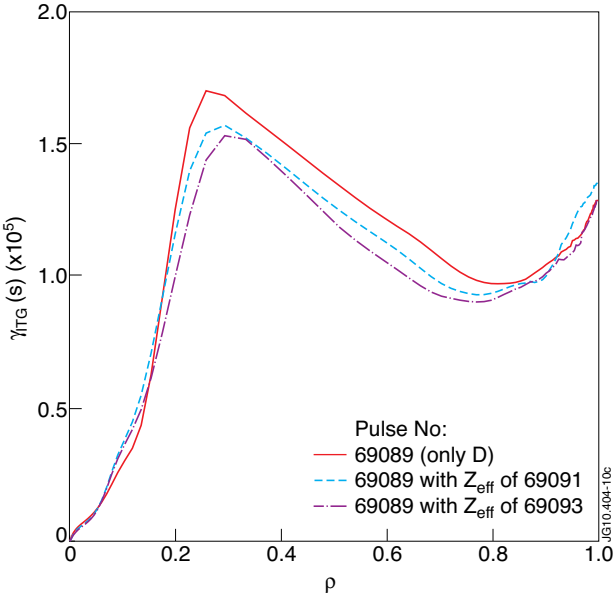

Figure 10: ITG growth rate as a function of the normalized toroidal flux coordinate, ρ, calculated by RITM code for the three discharges: (solid line) discharge 69089, (dashed line) discharge 69089 with Z_{eff} from 69091, and (dashed dotted line) discharge 69089 with Z_{eff} from 69093, shown in figure 9 by a red star, a crayon diamond and pink diamond, respectively.

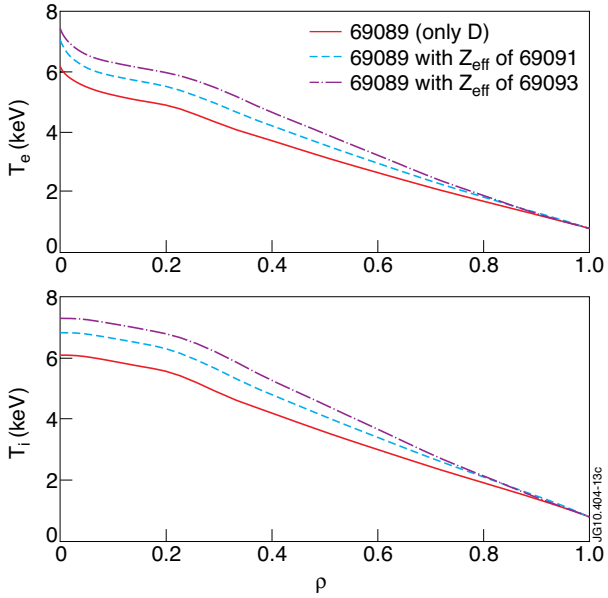

Figure 11: Electron (top) and ion (bottom) temperature profiles as functions of the normalized toroidal flux coordinate, ρ, (solid line) for 69089, (dashed line) for 69089 with Z_{eff} increased to that from 69091, and (dashed dotted line) for 69089 with Z_{eff} increased to that from 69093, corresponding to the the red star, the crayon and pink diamonds in figure 9, respectively.line) and 69093 (dashed dotted line).

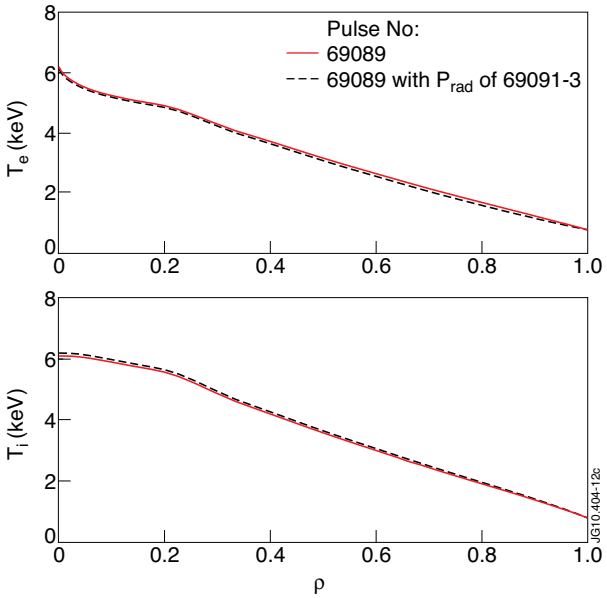

Figure 12: Electron (top) and ion (bottom) temperature profiles as functions of the normalized toroidal flux coordinate, ρ, (solid line) for 69089, and (dashed line) for 69089 with P_{rad}^{inLCFS} increased to that from 69091 – 3, corresponding to the red star and orange diamond in figure 9.

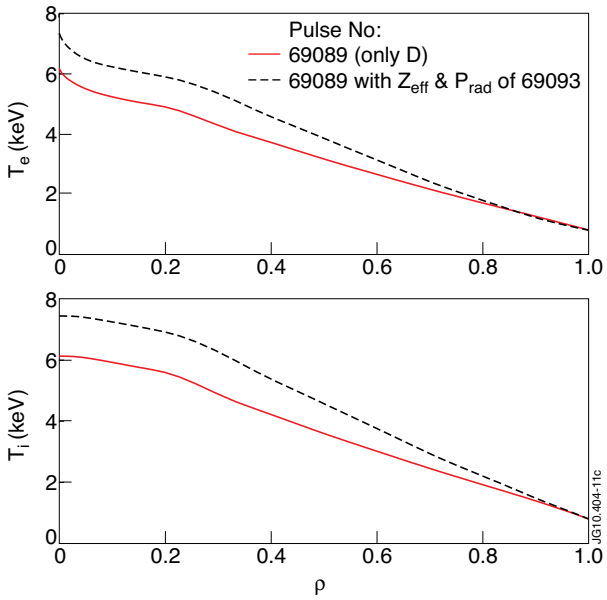

Figure 13: Electron (top) and ion (bottom) temperature profiles as functions of the normalized toroidal flux coordinate, ρ, (solid line) for Pulse No: 69089, and (dashed line) for Pulse No: 69089 with P_{rad}^{inLCFS} + Z_{eff} increased to that from Pulse No: 69093, corresponding to the red star and brown diamond in figure 9.